PCCP

PAPER

View Article Online
View Journal | View Issue

Cite this: *Phys. Chem. Chem. Phys.*, 2023, **25**, 3502

Aromatic heterocyclic anion based ionic liquids and electrolytes†

Mukhtiar Ahmed,[a] Soniya S. Rao,[b] Andrei Filippov,[a] Patrik Johansson *[b] and Faiz Ullah Shah *[a]

Received 10th November 2022,
Accepted 2nd January 2023

DOI: 10.1039/d2cp05272e

rsc.li/pccp

Five new ionic materials comprising fluorine-free aromatic heterocyclic anions based on pyridine and pyrazine combined with a common *n*-tetrabutylphosphonium cation, $(P_{4444})^+$, result in two room temperature ionic liquids (RTILs), one semi-solid, and two organic ionic plastic crystals (OIPCs) with melting points >20 °C. The OIPCs showed a plastic crystalline phase, multiple solid–solid transitions, and plastic crystalline and melt phases. For both the neat RTILs and the Li^+ conducting electrolytes, the nature and strength of the ion–ion interactions mainly depend on the position of the nitrogen atom with respect to the carboxylate group in the anions. Furthermore, for the RTILs the ionic conductivity is effected by the electronic structure and flexibility of the ions and the anions diffuse faster than the $(P_{4444})^+$ cation, but are slowed down in the electrolytes due to the strong electrostatic interactions between the carboxylate group of the anions and the Li^+, as shown both experimentally and computationally. Overall, this study describes the effect of structural tuning of aromatic anions on the ion–ion interactions and introduces new ionic materials with promising properties to be used as solid and liquid electrolytes in energy storage devices.

Introduction

Since their introduction by Sony in 1990, lithium-ion batteries (LIBs) have acquired a sizable market share.[1,2] They have the best energy densities, a high open circuit voltage, a low self-discharge rate, no memory effect, and a slow loss of charge when not in use. These properties make them the most popular rechargeable batteries for portable gadgets, electric vehicles and aerospace applications.[3,4] They do, however, have serious safety issues due to the electrolytes made up of fluorinated salts dissolved in flammable organic solvents.[5,6] Several attempts have been made to use nonflammable solvents, thermally and electrochemically stable (non-fluorinated) Li-salts, as well as additives to improve safety.[7–12] There is an urge to develop new salts and solvents with beneficial physical and chemical properties that can potentially replace the conventional fluorinated electrolytes.

Electrolytes based on ionic liquids (ILs) in general offer a range of suitable advantages[13–15] including low volatility and high thermal and electrochemical stabilities, inherent ionic conductivity, and can additionally be made task-specific and fluorine-free.[16,17] In general, their physicochemical properties are determined by the interactions between the cations and anions, which are controlled by the chemical functionalities present, with vast freedom in structural design to reduce these interactions and enhance ion mobilities.[18] In this context, there is a great potential to design and develop new fluorine-free anions that when combined with conventional cations could provide the desired physico-chemical and electrochemical properties.

Over the last two decades, extensive studies have been reported on the physicochemical and transport properties of various ILs and IL-based electrolytes.[19,20] However, a systematic relationship between the chemical structures or different combination of ions and the key physicochemical features of ILs is rarely reported.[21] The structural optimization of an anion is critical to control the thermal and electrochemical stabilities as well as ionic mobility, the latter has a substantial impact on the overall properties of an electrolyte.[22] In addition, the mobility of Li^+ through the solvent matrix and eventually into the electrode structure is determined by the nature of charge, charge distribution, and the geometry of the anions.[23] Most of the studies on ILs and IL-based electrolytes reported today are based on fluorinated anions, *i.e.* bis(trifluoromethanesulfonyl)-imide $(TFSI)^-$[24] and bis(fluorosulfonyl)imide $(FSI)^-$[25] anions. The fluorinated ILs and their electrolytes cause environmental problems not only during the synthesis but also at the recycling stages.

[a] *Chemistry of Interfaces, Luleå University of Technology, SE-971 87 Luleå, Sweden. E-mail: faiz.ullah@ltu.se*
[b] *Department of Physics, Chalmers University of Technology, SE-412 96 Gothenburg, Sweden. E-mail: patrik.johansson@chalmers.se*

† Electronic supplementary information (ESI) available. See DOI: https://doi.org/10.1039/d2cp05272e

This issue has sparked research into the design and development of new fluorine-free ILs and electrolytes.

Despite the huge potential to create new anions and combine with different cations to get new ILs with desired properties, the enormous number of possible anions is yet to synthesize and investigate. In this work, we investigate the effect of structural variations in novel ionic materials derived from nicotinic acid more commonly known as niacin, a form of vitamin B_3.[26,27] Nicotinic acid is chosen due to its sustainable nature, and the small and compact structure of the anion. In addition, structural analogues of nicotinic acid are selected for a systematic comparison, all the anions are based on six-membered aromatic nitrogen heterocycles and coupled with a common tetra(*n*-butylphosphonium) cation $(P_{4444})^+$. Doping of the ILs with the analogous lithium salts renders Li^+ conducting electrolytes. Both the neat ILs and the electrolytes are studied experimentally and computationally with respect to basic physicochemical properties such as ionic interactions and mobilities as well as electrochemical properties. While we here focus on the use as battery electrolyte solvents, these ILs could also be used as electrolytes for supercapacitors[28] as well as possibly as solvents for various tasks.[29]

Experimental

Materials

2-Picolic acid (2-PyrA), nicotinic acid (3-PyrA), *iso*nicotinic acid (4-PyrA), pyrazinoic acid (2,5-PyrA), 2,6-pyridinedicarboxylic acid (Pyr-2,6-diA), an aqueous solution of tetrabutylphosphonium hydroxide (40 wt% in water), and lithium hydroxide monohydrate (ACS reagents, >98% purity) were all received from Sigma-Aldrich and used without further purification. Sodium sulphate, lithium bicarbonate ($LiHCO_3$), dichloromethane and diethyl ether were purchased from VWR (BDH) chemicals. Electrolytes were prepared by mixing 10 mol% of Li(3-PyrA) and Li(2,5-PyrA) in the corresponding RTILs (for concentrations >10 mol% phase separation was observed).

Synthesis

Ionic materials. An aqueous solution of tetrabutylphosphonium hydroxide (50 mmol) was added dropwise into a stirred aqueous solution of the acid (50 mmol in 50 mL of water) – thus in stoichiometric amounts. The reaction mixture was stirred at room temperature for 4 hours and the progress of the reaction was monitored *via* thin layer chromatography (TLC) and upon completion, water was removed under reduced pressure using a rotary evaporator. The products were washed three times with 50 mL diethyl ether before being dissolved in dichloromethane and dried with anhydrous sodium sulphate. Finally, the solution was filtered, the residual solvent was removed under reduced pressure, and the final products were dried in a vacuum oven at 80 °C for more than 4 days. All the products were separated into quantitative yields. After purification and drying; (P_{4444})(3-PyrA) and (P_{4444})(2,5-PyrA) were obtained as RTILs, (P_{4444})(4-PyrA) and (P_{4444})(Pyr-2,6-diA) solids, and (P_{4444})(2-PyrA) as a semi-solid. The water content was measured by Karl Fischer titration (using Metrohm 917 Coulometer, Switzerland) and was determined to be less than 60 ppm for all the synthesized ionic materials. The formation and purity of the synthesized ionic materials were assessed by mass spectrometry and multinuclear (^{1}H, ^{13}C, and ^{31}P) NMR spectroscopy.

Lithium salts. Lithium (Li) salts of nicotinic acid (3-PyrA) and pyrazinoic acid (2,5-PyrA) were prepared by direct neutralization of the acids with $LiHCO_3$. Under continuous stirring, aqueous solutions of the acids were treated with solid $LiHCO_3$ in small portions, until the generation of gas bubbles stopped. The salts were obtained in quantitative yields after lyophilization and subsequent drying in vacuum oven at 80 °C for more than 2 days.

Nuclear magnetic resonance spectroscopy. The structures and purity of all the synthesized compounds were confirmed by using a Bruker Ascend Aeon WB 400 (Bruker BioSpin AG, Fallanden, Switzerland) NMR spectrometer. $CDCl_3$ and D_2O were used as solvents for the ionic materials and the lithium salt, respectively. The working frequencies were 400.21 MHz for ^{1}H, 100.64 MHz for ^{13}C, 155.53 MHz for ^{7}Li and 162.01 MHz for ^{31}P. The ^{31}P and ^{7}Li NMR spectra were externally referenced using H_3PO_4 (85%, 0 ppm) and 1.0 M $LiCl_{(aq)}$, respectively. Data were processed using Bruker Topspin 3.5 software.

Thermal analysis. Thermogravimetric analysis (TGA) was performed using a PerkinElmer TGA 8000 under N_2 gas at a heating rate of 10 °C per min using *ca.* 2–4 mg samples. The onset of decomposition temperature, T_{onset}, was calculated from the intersection of the baseline weight and the tangent of the weight *versus* temperature curve using Pyris software. Differential scanning calorimetry (DSC) was performed using a PerkinElmer DSC 6000 on *ca.* 2–5 mg of the sample placed in an aluminium pan. DSC data were collected at a scanning rate of 5 °C min^{-1} for both cooling and heating traces ranging from −75 to 200 °C. To maintain an inert environment inside the sample chamber, dry N_2 gas was delivered at a constant flow rate of 20 mL min^{-1}. The glass transition temperature, T_g, was determined by using the inflection mid-point of the initial *S*-shaped transition slope and determined from the onset with the aid of Pyris software.

Electrochemical characterization. The electrochemical stability and ionic conductivity were determined using a Metrohm Autolab PGSTAT302N electrochemical workstation with a FRA32M module for impedance measurements, all of which were controlled by Nova 2.02 software. A sealed Microcell HC from RHD instruments was used to hold about 70 μL of the sample. To determine the electrochemical stability window (ESW), linear sweep voltammetry (LSV) was performed with a three-electrode setup: a Pt wire with a diameter of 0.25 mm as working electrode (WE), a Pt crucible as counter electrode (CE), as well as sample container, and an Ag wire coated with AgCl as a pseudo-reference electrode (RE). Both cathodic and anodic scans were recorded at a rate of 1 mV s^{-1}. The electrochemical potentials were calibrated using ferrocene (Fc) as internal reference and shifted using $E_{Li/Li^+} \approx E_{Fc/Fc^+} + 3.2$ V.[30] The ESW limits were defined by a 0.1 mA cm^{-2} cut-off current density.

The ionic conductivity was obtained from the impedance measurements performed in a frequency range from 1 Hz to 1 MHz with an AC voltage amplitude of 10 mV_{rms}. All the impedance spectra were measured during heating and cooling over a temperature range from −20 to 100 ± 0.1 °C and the obtained ionic conductivities during heating and cooling match very well (Fig. S21, ESI†), thus only heating cycle data are presented. A two-electrode configuration was employed for ionic conductivity measurements, with a Pt wire as WE and a 70 μL Pt crucible as a sample container, as well as CE. Prior to each measurement, both the electrodes were polished with a 0.25 m of Kemet diamond paste. The cell constant was calculated using a Metrohm 100 S cm^{-1} KCl standard solution (K_{cell} = 18.5396 cm^{-1}). The cell was thermally equilibrated for 10 minutes before recording the impedance spectra.

The ionic conductivities are further analyzed by fitting the ionic conductivity data to the following Vogel–Fulcher–Tammann (VFT) eqn (1).

$$\sigma = \sigma_0 \exp\left(\frac{-B}{(T - T_0)}\right) \quad (1)$$

where σ_0 is a pre-exponential factor, B is an empirical material-dependent fitting parameter related to the dynamic T_g and activation/pseudo activation energy (E_σ) of the system. The reference temperature T_0 is attributed to the ideal vitreous transition temperature, at which configurational entropy vanishes.[31] T_0 is determined by fitting the temperature-dependent conductivity data to the VTF equation for the best linearity relationship.

Pulsed field gradient diffusometry. NMR self-diffusion measurements were performed using a Bruker Ascend/Aeon WB 400 (Bruker BioSpin AG) NMR spectrometer with a resonance frequency of 400.27 MHz for ^{1}H and 155.56 MHz for ^{7}Li. Pulsed-Field Gradient (PFG) NMR self-diffusion measurements were performed on ^{1}H with a PFG NMR probe Diff50 (Bruker) with a maximum amplitude of the magnetic field gradient pulse of 29.73 T m^{-1}. The samples were placed in a standard 5 mm NMR glass tube and closed with a plastic stopper to avoid contact with air. Prior to measurements, each sample was equilibrated at a specific temperature for 30 min. The details of the PFG NMR technique for measuring molecular diffusion coefficients are available elsewhere.[32] The diffusion decay (DD) of amplitude A of the NMR spectral lines, obtained by Fourier transformation of a descending half of the stimulated-echo (StE), as a function of the amplitude of the applied pulsed field gradient. For the stimulated echo pulse sequence used, diffusion decay of A in the case of simple non-associating molecular liquid can be described by eqn (2):[33]

$$A(g,\delta,t_d) = A(0)\exp(-\gamma^2 g^2 \delta^2 D t_d) \quad (2)$$

where $A(0)$ is the factor proportional to the amount of magnetic nuclei, and to spin-lattice and spin-spin relaxation times, γ is the gyromagnetic ratio for a used nucleus; g and δ are the amplitude and duration of the gradient pulse; t_d is the diffusion time, and D is the self-diffusion coefficient. t_d was in the range from 4 to 100 ms for ^{1}H diffusion and from 5 to 15 ms for ^{7}Li diffusion. The diffusion experiments were performed in the temperature range from 295 to 373 K. No diffusion time dependence was observed in these measurements. Diffusional decays (DDs) for the neat ILs and the IL-based electrolytes have a single exponential form and are not affected by the diffusion time t_d. Experimental DDs are then fitted to eqn (2) to obtain the diffusion coefficients.

The ion diffusivity data for the neat ILs and the electrolytes are analyzed by using VFT eqn (3):

$$D = D_0 \exp\left(\frac{-B}{(T - T_0)}\right) \quad (3)$$

where D_0, T_0, B are adjustable parameters. Energy of activation for diffusion is related with B as $E_D = B \times R$. We have described $D(T)$ by fitting D_0, T_0 and B.

FTIR spectroscopy

Attenuated total reflection Fourier transform infrared (ATR-FTIR) spectra were recorded using a Bruker IFS 80v spectrometer equipped with a deuterated triglycine sulfate (DTGS) detector and diamond ATR accessory, employing the double-side forward–backward acquisition mode. The total number of scans was 256, co-added and signal-averaged at an optical resolution of 4 cm^{-1}.

Computational studies

Geometry optimized structures of the 2-PyrA, 3-PyrA, 4-PyrA, and 2,5-PyrA and Li^+ ion–pairs with interactions by the carboxyl group (Fig. 8 and Fig. S23, ESI†), were obtained by density functional theory (DFT) calculations employing the M06-2X functional[34,35] and the 6-311+(d,p) basis set using Gaussian-16.[36–38] The structures were verified to be minima by calculating the second derivatives of the energy with respect to nuclear displacements. The ultrafine grid option was used in all cases.

To gain further insight into the role of the charge distribution the donor–acceptor interactions were evaluated using Natural Bonding Orbitals (NBOs)[39] and the second-order Fock matrix (Tables S4–S7, ESI†). The stabilization energy E^{35} associated with donor NBO(i) and acceptor NBO(j) was computed by eqn (4):

$$E^{(2)} = \Delta E_{ij} = q_i\left(\frac{(F(i,j))^2}{\varepsilon_j - \varepsilon_i}\right) \quad (4)$$

where q_i is the orbital occupancy, ε_i and ε_j are diagonal elements (orbital energies) and $F_{(i,j)}$ is the off-diagonal NBO Fock matrix element.

Results and discussions

We start with a brief description of the five ionic materials, followed by thermal properties assessment and the effect of anion chemistry on the thermal stability of the synthesized ionic materials. The ionic materials and the IL electrolytes were further assessed for LIB-relevant properties such as ionic conductivity, ion diffusion, and electrochemical stability before

progressing to FTIR spectroscopy, variable-temperature line width and chemical shift analysis and computational studies to further decipher the coordination and ion–ion interactions.

Basics of synthesized ionic materials

The chemical structures of the ionic materials (Scheme 1) agree well with the NMR analysis (Fig. S1–S15, ESI†) as well as the mass spectra (Fig. S16–S20, ESI†) shown in the ESI.† First, the aliphatic alkyl chains attached to the $(P_{4444})^+$ cation show distinct resonance lines in the ^{1}H NMR spectrum a triplet at 0.93 ppm for the terminal methyl groups, a multiplet 1.46–1.54 ppm for the methylene protons, and another multiplet 2.39–2.46 ppm for the eight protons of the carbon atoms directly attached to the phosphorous atom. Second, the presence of aromatic resonance lines, 6.5–8.5 ppm, and the lack of the broad resonance line for any acidic proton corroborated the deprotonation of the acids (Fig. S1–S5, ESI†). Third, the aliphatic carbon atoms display characteristic resonance lines in the region 13–24 ppm in the ^{13}C NMR spectra (Fig. S6–S10, ESI†), while those of the carboxylate groups in the anions are found in the range 168–171 ppm. Finally, the ^{31}P NMR spectra indicate a single resonance line at *ca.* 33 ppm (Fig. S11–S15, ESI†).

Turning to the aggregation states of the five systems (P_{4444})(3-PyrA) and (P_{4444})(2,5-PyrA) are RTILs, (P_{4444})(2-PyrA) is a semi-solid, while $(P_{4444})_2$(Pyr-2,6-diA) and (P_{4444})(4-PyrA) are solids. The latter can arguably be due to stronger interionic interactions as well as the comparatively more symmetric $(4\text{-PyrA})^-$ and $(\text{Pyr-2,6-diA})^-$ anions, as symmetry is known to facilitate crystallinity.[40–42]

Thermal properties

The thermal stability of the neat ILs having a common *n*-butylphosphonium cation is ranging from 245 °C to 330 °C, mainly depending on the nature of the anion (Fig. 1a and Table 1). The order of thermal stability decrease as: (P_{4444})(3-PyrA) > (P_{4444})(4-PyrA) > (P_{4444})(2,5-PyrA) > (P_{4444})(2-PyrA) > $(P_{4444})_2$(Pyr-2,6-diA) and increases as the delocalization of the negative charge on the anion increases. The (P_{4444})(3-PyrA) IL thermal stability *vs.* the (P_{4444})(4-PyrA) and (P_{4444})(2-PyrA) ILs might be explained by the negative inductive and positive resonance effects (electron-donating effect) of the pyridine nitrogen, which can cause an extended delocalization of electrons lead to a more polarizable structure resulting in thermally stable anion (Scheme 2).[43–45] In the case of (P_{4444})(2,5-PyrA), the presence of an extra nitrogen atom at 5-position neutralizes the electron withdrawing effect generated by the nitrogen at 2-position and stabilizes the anion to a greater extent as compared to the anion in (P_{4444})(2-PyrA).

The thermal stabilities of these new ILs are quite comparable to previous phosphonium-based halogen-free ILs.[46,47] The thermal stabilities of the Li-salts are substantially higher, by almost 100 °C, than the neat ILs, which is attributed to the strong Li^+ electrostatic interaction with the anions, and the higher thermal stability of the Li^+ cation than the organic cation $(P_{4444})^+$. As a consequence, the thermal stabilities are slightly improved for the electrolytes as compared to the neat ILs (Fig. 1b and Table 1).

Although the chemical structures of all the ionic materials are quite similar, their thermal behavior is completely different. The multiple solid–solid phase transitions observed for (P_{4444})(4-PyrA) and $(P_{4444})_2$(Pyr-2,6-diA) indicate typical OIPC behavior (Fig. 2 and Table 1).[48,49] Before melting, (P_{4444})(4-PyrA) exhibits rich phase behavior with multiple solid–solid phase transitions, which cannot be due to the breakdown at these temperatures as confirmed by the TGA data (Fig. 1). These solid–solid transitions show progressive transformation of material from an ordered phase into a disordered phase, leading to higher plasticity and ion mobility.[50]

Upon heating $(P_{4444})_2$(Pyr-2,6-diA) passes from a glassy state to a subcooled liquid phase, and then a cold crystallization occurs, followed by a melting transition. A very similar thermal behavior is exhibited by the neat (P_{4444})(3-PyrA) but in a much lower temperature range. This type of behavior is common for many polymers and other amorphous compounds.[51,52] The neat (P_{4444})(2-PyrA) and (P_{4444})(2,5-PyrA) exhibit only glass transitions.

The addition of 10 mol% of Li(3-PyrA) salt to (P_{4444})(3-PyrA) slightly shifts the glass transition temperature, while both the crystallization and melting peaks disappear, and hence the electrolyte behaves as a pure glass-forming liquid. This is associated with the smaller radius of Li^+, causing increases in the ionic strength and/or ion–ion interactions.[53] and a similar change for the (P_{4444})(2,5-PyrA) based electrolyte.

Ionic conductivity

The neat (P_{4444})(3-PyrA) IL and its electrolyte shows higher ionic conductivities independent of temperature range as compared with the neat (P_{4444})(2,5-PyrA) IL and the corresponding electrolyte (Fig. 3). This can be linked to the influence of electronic structure and flexibility of the ions generated by geometry variations possibly including steric hindrances. In the case of

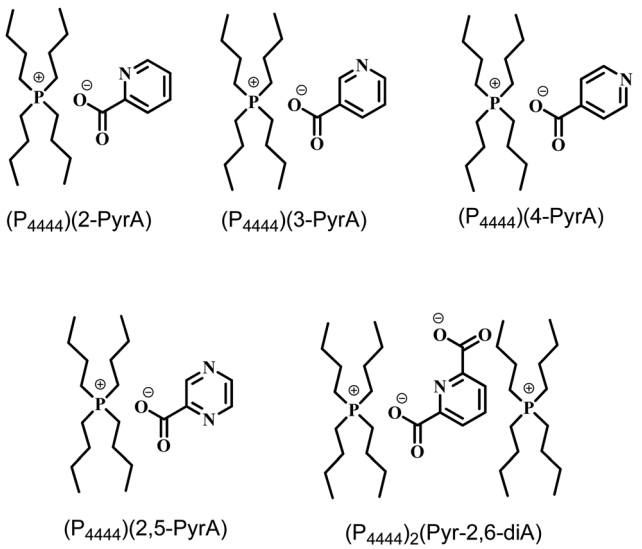

Scheme 1 Chemical structures and abbreviations of the five ionic materials.

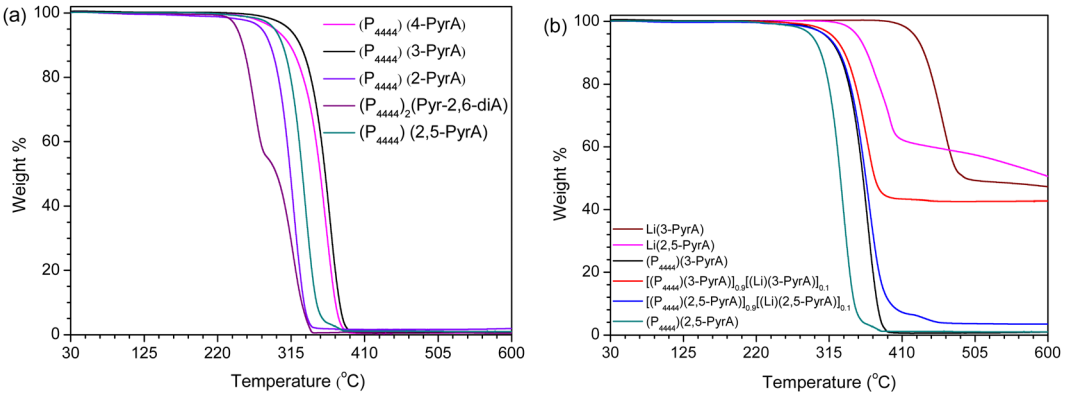

Fig. 1 TGA thermograms of the neat ILs (a) and the Li(3-PyrA), Li(2,5-PyrA) salts and the $[(Li)(3\text{-PyrA})]_{0.1}[(P_{4444})(3\text{-PyrA})]_{0.9}$ and $[(Li)(2,5\text{-PyrA})]_{0.1}[(P_{4444})(2,5\text{-PyrA})]_{0.9}$ electrolytes (b).

Table 1 Physiochemical properties of the synthesized ionic materials and the electrolytes[a]

System	T_g (°C)	T_c (°C)	T_m (°C)	T_{s-s} (°C)	T_d (°C)	σ (S cm^{-1})
(P_{4444})(2-PyrA)	−57	—	—	—	291	—
(P_{4444})(3-PyrA)	−53	−15	31	—	332	1.00×10^{-4}
(P_{4444})(4-PyrA)	−35	—	42	−9, 2, 36	317	—
(P_{4444})(2,5-PyrA)	−55	—	—	—	303	7.83×10^{-6}
$(P_{4444})_2$(Pyr-2,6-diA)	−16	31	118		245	—
$[(P_{4444})(3\text{-PyrA})]_{0.9}[Li(3\text{-PyrA})]_{0.1}$	−55	—	—	—	335	7.47×10^{-5}
$[(P_{4444})(2,5\text{-PyrA})]_{0.9}[Li(2,5\text{-PyrA})]_{0.1}$	−57	—	—	—	330	7.73×10^{-6}

[a] T_g: glass transition, T_c: cold crystallization, T_m: melting point, T_d: decomposition temperature, T_{s-s}: solid state transition, σ: ionic conductivity at 20 °C.

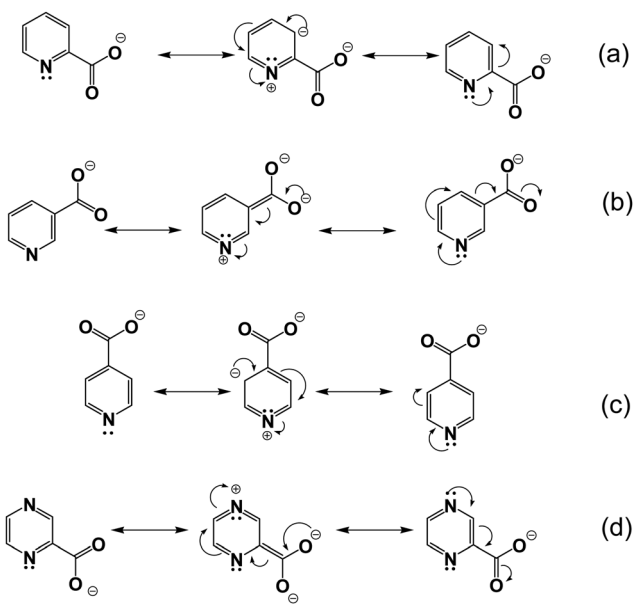

Scheme 2 Resonance structures of (a) $(2\text{-PyrA})^-$, (b) $(3\text{-PyrA})^-$, (c) $(4\text{-PyrA})^-$ and (d) $(2,5\text{-PyrA})^-$ anions.

(P_{4444})(3-PyrA), the negative inductive and positive resonance effects in the anion reduces the ionic interactions. In general, ionic conductivities of ILs slightly decrease upon addition of Li-salt due to increased Coulombic interactions leading to formation of aggregates, reduced free volume, and charge carrier concentration,[54] and has also been observed previously for $(P_{4444})^+$ based electrolytes.[16,55]

By a VFT fitting procedure of these data, the E_σ of (P_{4444})(2,5-PyrA) is determined to be slightly larger than for (P_{4444})(3-PyrA) (Table S1, ESI†), and even larger for the electrolytes, as expected from the relatively stronger ion–ion interactions. Furthermore, as expected, T_0 are *ca.* 50 K below T_g and also agree well with the empirical approximation of IL based electrolytes: $T_0/T_g \approx 0.75$.[56]

NMR diffusometry

The PFG NMR diffusometry derived ion diffusion coefficients exhibit monotonic increase as a function of temperature (Fig. 4 and Table S2, ESI†). For the ILs the anions diffuse faster than the cations, which is directly related to the ion sizes. The $(2,5\text{-PyrA})^-$ anion diffuses slower than the $(3\text{-PyrA})^-$ anion, which is due the presence of an extra nitrogen atom in the aromatic ring, which not only increases the ionic mass but also contributes to stronger ionic interactions. In agreement with the conductivity data above, the diffusivities of both cations and anions reduce in the electrolytes, and despite having the lowest mass and smallest radius, the Li^+ cation diffuses the slowest, and in particular at lower temperatures, suggesting temperature dependent interactions with the anions.

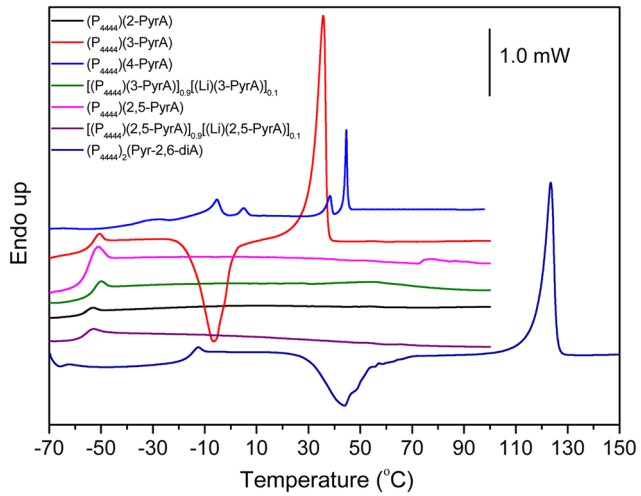

Fig. 2 DSC traces for the neat ionic materials and the electrolytes.

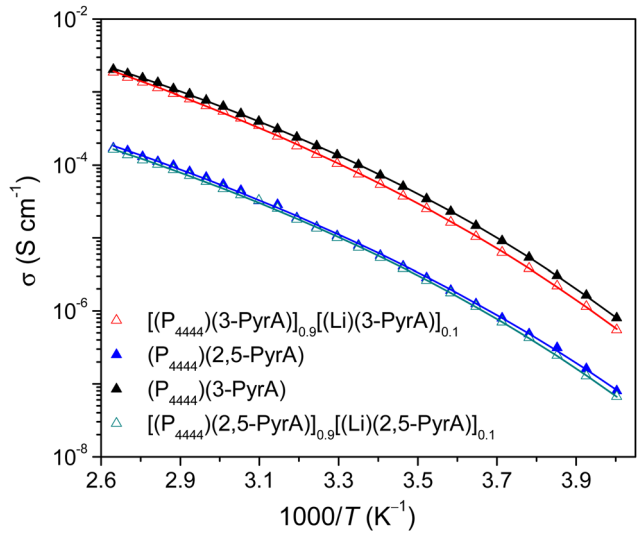

Fig. 3 Ionic conductivity as a function of temperature for the neat ILs and the electrolytes. The solid lines indicate best fit of the data to the VFT equation.

VFT fits of the diffusivity data result in parameters comparable for the cations and anions of the ILs, but with marked difference for the electrolytes (Fig. 4 and Table S2, ESI†) The former can be understood as diffusion in a homogeneous matrix, primarily determined by the free volume available.[57] The latter is a consequence of increased ion–ion interactions, here manifested as a slightly changed apparent activation energy, E_D, as well as in D_0. As a sidenote, the T_0 from the ionic conductivity data are lower than the T_0 from the diffusivity data; the latter is an average of the diffusion coefficients of isolated, paired, and clustered ions, regardless of charge, whereas the former only has contributions from charged species.

^{7}Li and ^{31}P NMR spectroscopy

The full width at half-maximum (fwhm) analysis show these to initially increase as a function of temperature and subsequently decrease continuously, suggesting limited ion mobility at slightly elevated temperatures (Fig. 5a and Fig. S22, ESI†), likely from ion pairing, aggregation and inhomogeneity in the systems.[58] The line broadening at lower temperatures is more pronounced for the $[(P_{4444})(2,5\text{-PyrA})]_{0.9}[(Li)(2,5\text{-PyrA})]_{0.1}$ electrolyte than the $[(P_{4444})(3\text{-PyrA})]_{0.9}[(Li)(3\text{-PyrA})]_{0.1}$ electrolyte, which might be due to the formation of thermodynamically stable aggregates in the former. This can be explained to be due to the presence of nitrogen atom in the anion aromatic ring, facilitating stronger coordination of Li^+ with the carboxylate group of the $(3\text{-PyrA})^-$ anion, in agreement with the ionic conductivity data. The slight up field chemical shift in the ^{7}Li NMR spectra as a function of temperature suggests change in chemical environment of the Li^+ ion (Fig. 5b). This change in chemical shift points towards weaker interactions between the Li^+ ions and the aromatic anions and enhanced ion mobility at elevated temperatures.

Electrochemical stability

By LSV the ESWs are found to be 3.57 and 2.82 V for the $(P_{4444})(3\text{-PyrA})$ and $(P_{4444})(2,5\text{-PyrA})$ ILs, respectively (Fig. 6 and Table S3, ESI†), clearly superior to previously reported

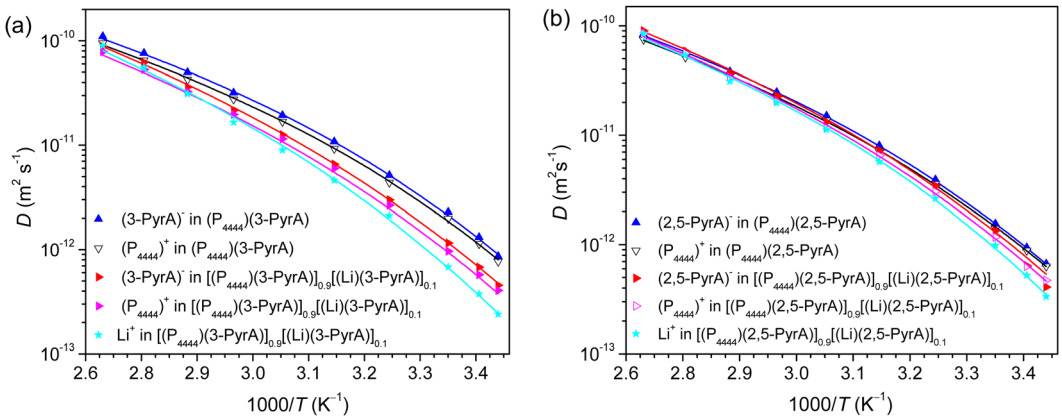

Fig. 4 Diffusion coefficients of ions in the (a) neat $(P_{4444})(3\text{-PyrA})$ IL and its electrolyte and (b) neat $(P_{4444})(2,5\text{-PyrA})$ IL and its electrolyte. Symbols indicate the experimental data and the solid lines represent the VFT fittings.

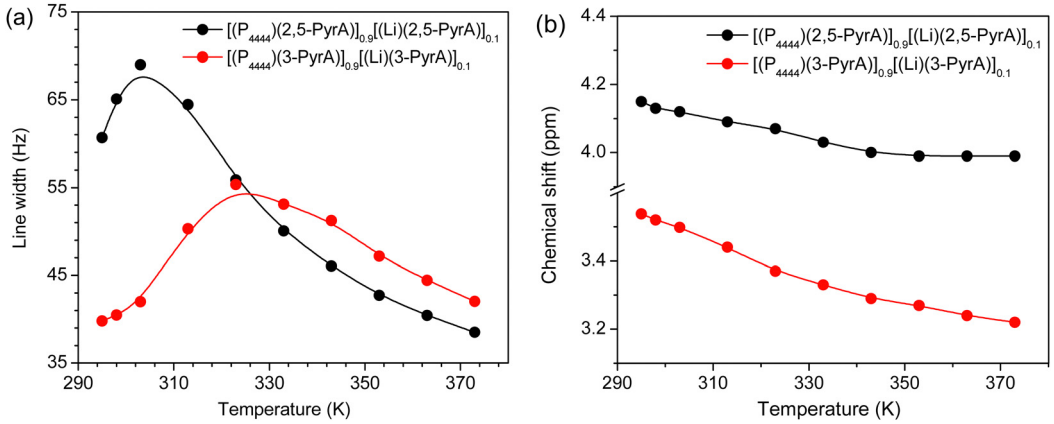

Fig. 5 Line width (a) and chemical shift (b) of ^{7}Li NMR spectra of the electrolytes as a function of temperature.

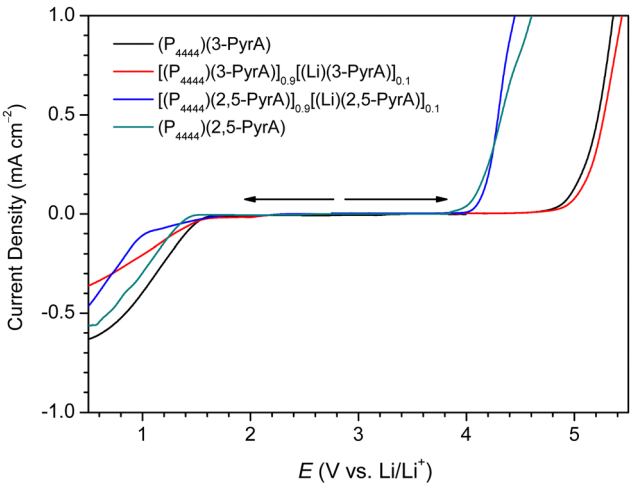

Fig. 6 LSV curves of the neat ILs and the electrolytes using GC as the WE.

similar heterocyclic based halogen-free ILs.[59] The ESWs of their electrolytes are slightly improved and this can possibly be attributed to the formation of a passivating layer on the surface of the WE.[60,61]

The wider ESW of the (P_{4444})(3-PyrA) IL can be explained by the extensive electron polarization and weak ionic interactions, enabling the $(P_{4444})^{+}$ cation to possibly house incoming electrons and thereby expand the anodic limit (Scheme 2). The relatively lower anodic limit of the (P_{4444})(2,5-PyrA) IL might be due to the presence of two N atoms, as opposed to one N atom in $(3\text{-PyrA})^{-}$, in the aromatic ring of $(2,5\text{-PyrA})^{-}$, which are more susceptible to oxidation.[62] On the cathodic scans, both the neat ILs and the electrolytes reveal continuous reduction *ca.* 1 V (*vs.* Li/Li^{+}), which is due the presence of acidic alpha methylene protons in the $(P_{4444})^{+}$ cation.[51,57,58]

FTIR spectroscopy

For both the (P_{4444})(3-PyrA) and the (P_{4444})(2,5-PyrA) ILs, the prominent single strong infrared bands centered at 1603 cm^{-1} and 1615 cm^{-1} with shoulders (Fig. 7), suggest a single mode of cation–anion interaction, indicating a localized negative charge on one of the oxygen atoms similar to a carbonyl group.[63] The symmetric stretching band of the carboxylate group appears as a single and symmetrical peak at *ca.* 1350 cm^{-1} for (P_{4444})(3-PyrA) and (P_{4444})(2,5-PyrA) ILs again indicates one kind of ionic interaction and presumably justifies the low melting point of these materials – rendering them RTILs. For the other ionic materials, (P_{4444})(2-PyrA), (P_{4444})(4-PyrA) and $(P_{4444})_2$(Pyr-2,6-diA), the broad and weak asymmetric stretching (1570–1615 cm^{-1}) and the symmetric stretching bands (1320–1370 cm^{-1}) appear in the lower wavenumber regions, behaving as carboxylate groups with delocalized negative charge on the two oxygen atoms and suggest the presence of long range strong ionic interactions, correlating with their solid/semi-solid state.

The modes of cation–anion interactions change for the electrolytes, where new asymmetric stretching bands at 1380 and 1400 cm^{-1} appear (Fig. 7d), alongside a significant broadening of the asymmetric band at 1615 cm^{-1} with distinct shoulders at both sides. This clearly suggests the interaction of the Li^{+} ions with the carboxylate groups of the anions.

The ionic interactions in these analogous ionic materials are primarily determined by their anion chemistry. The position of nitrogen atom in the aromatic ring with respect to the carboxyl group plays a critical role in controlling the electron delocalization and, thus, the ionic interactions. Nitrogen atom being more electronegative than carbon atom extract electrons *via* the negative inductive effect, while the lone pair of electrons on nitrogen allows electrons donation through a resonance effect (Scheme 2). At the 3 position, nitrogen may contribute a pair of electrons and raise the polarity of the anions *via* push–pull effects, as well as enhance the aromatic nature of the anions to stabilize them, as confirmed by the higher stability of (P_{4444})(3-Pyr). Additionally, the resonance effect of nitrogen atom can enhance the carbonyl-like character of the carboxy group, as revealed by the FTIR spectra of the (P_{4444})(3-Pyr) and (P_{4444})(2,5-Pyr). This in turn reduces the ionic contacts with the counter cation, rendering room temperature liquid salts. The resonance effect of nitrogen atom increases the electron density around the carboxyl group and increase the strength of ionic interactions, as

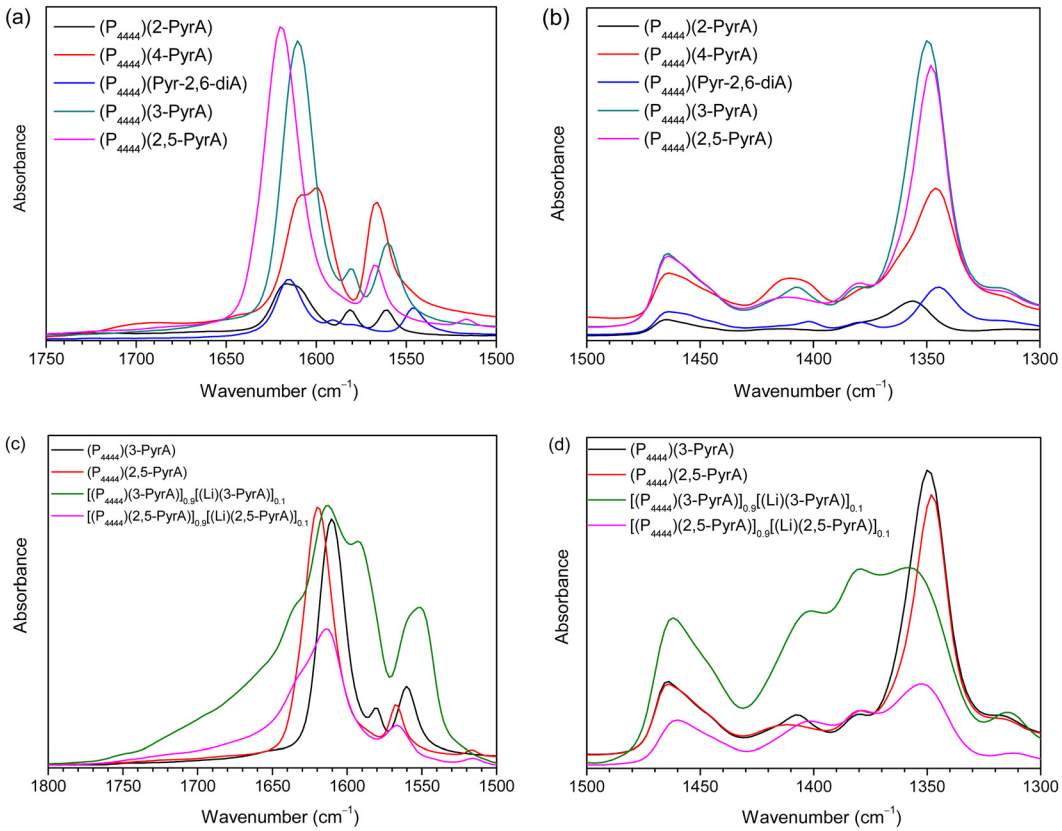

Fig. 7 FTIR spectra of (a and b) the neat ILs and (c and d) the electrolytes.

observed in the case of ambient temperature solid or semi-solid ionic materials (P_{4444})(2-Pyr) and (P_{4444})(4-Pyr).

Ion–pair interaction energies and NBO

Both the (2-PyrA)$^-$ and the (2,5-PyrA)$^-$ anions interact with the Li^+ cations *via* both the ring nitrogen atom (N1) and the carboxylate group (Fig. 8 and Fig. S23, ESI†), while the other two anions interact only by the carboxylate group. Overall, the interaction energies follow the order: (2-PyrA)$^-$ > (2,5-PyrA)$^-$ > (3-PyrA)$^-$ > (4-PyrA)$^-$.

In more detail, the stabilization energies and the NBO analysis foremost show strong interactions between the donor lone pairs (LP) of N1 and the antibonding acceptor π *C1–C2 (or C3–C4) orbitals within the aromatic ring for all anions (Tables S4–S7, ESI†). The charge transfer from the aromatic ring to the carboxylate group is evident through σ C1–N1 → π* Ca═O1 delocalization. At the same time, the extension of delocalization of electrons in (3-PyrA)$^-$ is evident through the significant σ C4–C3 → π *Ca═O2 delocalization leading to a more polarizable structure (Table S5, ESI†). Thus, *σ*-induction combined with π-delocalization results in significant push–pull effects on the electron density and delocalization.

Turning to the ion–pairs the electron delocalization within the aromatic ring, both σ C5–N1 → π* C1–C2 and σ C5–N1 → π*C4–C5

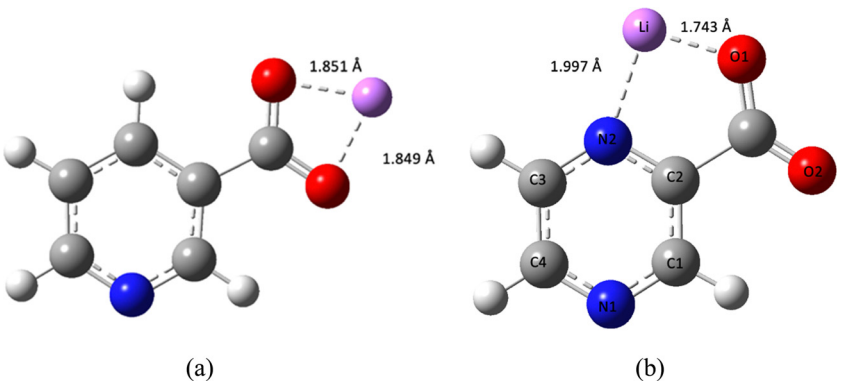

Fig. 8 Optimized geometries of (a) Li^+–(3-PyrA)$^-$ and (b) Li^+–(2,5-PyrA)$^-$ ion–pairs including coordination bond distances.

increase significantly for Li^+–(2-PyrA)$^-$ (Table S4, ESI†). In contrast, the presence of an extra ring nitrogen atom in (2,5-PyrA)$^-$ anion largely neutralizes the electron withdrawing effect of N1 and thereby stabilizes the anion, but again the ion–pair shows increased hyper-conjugative interactions (Table S7, ESI†). The Li^+–(3PyrA)$^-$ ion pair shows significantly higher σ C3–N1 → σ *C3–C4 delocalization within the ring on Li^+ association compared to the other anions. Overall, comparing the two (P_{4444})(3-PyrA) and (P_{4444})(2,5-PyrA) RTILs, lower interaction energies of Li^+–(3-PyrA)$^-$ anion and higher delocalization of negative charges compared to (2,5-PyrA)$^-$ anion.

Conclusions

The change in position of the nitrogen atom in these N-containing aromatic heterocyclic anions has dramatically affect the ionic interactions and the overall physiochemical properties of the ionic materials, ranging from RTILs to semi solid and OIPCs. Among all these ionic materials, the (P_{4444})(3-PyrA) RTIL and its electrolyte having anion with a nitrogen atom at 3 position has superior thermal and electrochemical stabilities, higher ionic conductivity and ion diffusivity. As expected, Li^+ ions diffused slowest in both the electrolytes revealing inhomogeneous aggregate formation *via* stronger electrostatic interactions between Li^+ ions and the aromatic heterocyclic anions, as confirmed by NMR (^{7}Li and ^{31}P) and FTIR spectroscopic data, and computational studies. Altogether, the neat (P_{4444})(3-PyrA) IL and its electrolyte, the anion of which is derived from niacin (a form of vitamin B_3), provide promising physicochemical properties to be used as a liquid electrolyte in energy storage devices.

Author contributions

Mukhtiar Ahmed: synthesis, methodology, characterization, writing original draft. Soniya Rao: DFT calculations, editing. Andrei Filippov: NMR diffusometry, conceptualization, editing. Patrik Johansson: supervision, conceptualization, methodology, editing. Faiz Ullah Shah: supervision, conceptualization, methodology, editing.

Conflicts of interest

There are no conflicts to declare.

Acknowledgements

The financial support from the Swedish Energy Agency (project number: 48194-1) is gratefully acknowledged. SR and PJ are in addition grateful for the computational resources provided by the Swedish National Infrastructure for Computing (SNIC) at Chalmers Centre for Computational Science and Engineering (C3SE)/e-commons and the National Supercomputing Centre (NSC).

References

1 M. Li, J. Lu, Z. Chen and K. Amine, 30 years of lithium-ion batteries, *Adv. Mater.*, 2018, **30**, 1800561.
2 T. Nagaura, Lithium ion rechargeable battery, *Prog. Batteries Sol. Cells*, 1990, **9**, 209.
3 X. Tian, Y. Yi, B. Fang, P. Yang, T. Wang, P. Liu, L. Qu, M. Li and S. Zhang, Design strategies of safe electrolytes for preventing thermal runaway in lithium ion batteries, *Chem. Mater.*, 2020, **32**, 9821.
4 M. A. Navarra, A. Tsurumaki, F. M. Vitucci, A. Paolone, O. Palumbo, S. Panero and A. Novel, Li^+-Conducting Polymer Membrane Gelled by Fluorine-Free Electrolyte Solutions for Li-Ion Batteries, *Batteries Supercaps*, 2020, **3**, 1112.
5 Q. Wang, B. Mao, S. I. Stoliarov and J. Sun, A review of lithium ion battery failure mechanisms and fire prevention strategies, *Prog. Energy Combust. Sci.*, 2019, **73**, 95.
6 Q. Li, J. Chen, L. Fan, X. Kong and Y. Lu, Progress in electrolytes for rechargeable Li-based batteries and beyond, *Green Energy Environ.*, 2016, **1**, 18.
7 Z. Zeng, V. Murugesan, K. S. Han, X. Jiang, Y. Cao, L. Xiao, X. Ai, H. Yang, J. G. Zhang and M. L. Sushko, Non-flammable electrolytes with high salt-to-solvent ratios for Li-ion and Li-metal batteries, *Nat. Energy*, 2018, **3**, 674.
8 H. Q. Pham, H. Y. Lee, E. H. Hwang, Y. G. Kwon and S. W. Song, Non-flammable organic liquid electrolyte for high-safety and high-energy density Li-ion batteries, *J. Power Sources*, 2018, **404**, 13.
9 X. Liu, X. Shen, F. Zhong, X. Feng, W. Chen, X. Ai, H. Yang and Y. Cao, Enabling electrochemical compatibility of non-flammable phosphate electrolytes for lithium-ion batteries by tuning their molar ratios of salt to solvent, *Chem. Commun.*, 2020, **56**, 6559.
10 D. Ding, Y. Maeyoshi, M. Kubota, J. Wakasugi, K. Kanamura and H. Abe, Non-flammable super-concentrated polymer electrolyte with ''solvated ionic liquid'' for lithium-ion batteries, *J. Power Sources*, 2021, **506**, 230099.
11 N. von Aspern, M. Leissing, C. Wölke, D. Diddens, T. Kobayashi, M. Börner, O. Stubbmann-Kazakova, V. Kozel, G. V. Röschenthaler and J. Smiatek, Non-Flammable Fluorinated Phosphorus(III)-Based Electrolytes for Advanced Lithium-Ion Battery Performance, *ChemElectroChem*, 2020, **7**, 1499.
12 G. Kim, S. Jeong, M. Joost, E. Rocca, M. Winter, S. Passerini and A. Balducci, Use of natural binders and ionic liquid electrolytes for greener and safer lithium-ion batteries, *J. Power Sources*, 2011, **196**, 2187.
13 H. Nakagawa, Y. Fujino, S. Kozono, Y. Katayama, T. Nukuda, H. Sakaebe, H. Matsumoto and K. Tatsumi, Application of nonflammable electrolyte with room temperature ionic liquids (RTILs) for lithium-ion cells, *J. Power Sources*, 2007, **174**, 1021.
14 H. Lee, M. Yanilmaz, O. Toprakci, K. Fu and X. Zhang, A review of recent developments in membrane separators for rechargeable lithium-ion batteries, *Energy Environ. Sci.*, 2014, **7**, 3857.
15 S. Wilken, S. Xiong, J. Scheers, P. Jacobsson and P. Johansson, Ionic liquids in lithium battery electrolytes:

Composition versus safety and physical properties, *J. Power Sources*, 2015, **275**, 935.
16 F. U. Shah, O. I. Gnezdilov, I. A. Khan, A. Filippov, N. A. Slad and P. Johansson, Structural and ion dynamics in fluorine-free oligoether carboxylate ionic liquid-based electrolytes, *J. Phys. Chem. B*, 2020, **124**, 9690.
17 F. Ilyas, M. Ishaq, M. Jabeen, M. Saeed, A. Ihsan and M. Ahmed, Recent trends in the benign-by-design electrolytes for zinc batteries, *J. Mol. Liq.*, 2021, **343**, 117606.
18 Z. Lei, B. Chen, Y. M. Koo and D. R. MacFarlane, Introduction: ionic liquids, *Chem. Rev.*, 2017, **117**, 6633.
19 X. Chenxuan, G. Yang, D. Wu, M. Yao, C. Xing, J. Zhang and H. Zhang, *et al.*, Roadmap on ionic liquid electrolytes for energy storage devices, *Chem. – Asian J.*, 2021, **16**, 549–562.
20 A. Basile, M. Hilder, F. Makhlooghiazad, C. Pozo-Gonzalo, D. R. MacFarlane, P. C. Howlett and M. Forsyth, Ionic liquids and organic ionic plastic crystals: Advanced electrolytes for safer high performance sodium energy storage technologies, *Adv. Energy Mater.*, 2018, **8**, 1703491.
21 J. M. Slattery, C. Daguenet, P. J. Dyson, T. J. S. Schubert and I. Krossing, How to predict the physical properties of ionic liquids: a volume-based approach, *Angew. Chem., Int. Ed.*, 2007, **46**, 5384–5388.
22 M. Armand, P. Johansson, M. Bukowska, P. Szczeciński, L. Niedzicki, M. Marcinek, M. Dranka, J. Zachara, G. Żukowska, M. Marczewski, G. Schmidt and W. Wieczorek, Review—Development of Hückel type anions: from molecular modeling to industrial commercialization. A success story, *J. Electrochem. Soc.*, 2020, **167**, 070562.
23 T. Ruther, A. I. Bhatt, A. S. Best, K. R. Harris and A. F. Hollenkamp, Electrolytes for lithium (sodium) batteries based on ionic liquids: highlighting the key role played by the anion, *Batteries Supercaps*, 2020, **3**, 793–827.
24 D. R. MacFarlane, P. Meakin, J. Sun, N. Amini and M. Forsyth, Pyrrolidinium imides: a new family of molten salts and conductive plastic crystal phases, *J. Phys. Chem. B*, 1999, **103**, 4164–4170.
25 I. A. Shkrob, T. W. Marin, Y. Zhu and D. P. Abraham, Why bis(fluorosulfonyl)imide is a ''magic anion'' for electrochemistry, *J. Phys. Chem. C*, 2014, **118**, 19661–19671.
26 Y. Fan, W. Li, S. Zhang, S. Sun and L. Yang, Vitamin B_3-based protic ionic liquids as green solvents for the isolation of astilbin from rhizoma smilacis glabrae, *Ind. Crops Prod.*, 2020, **152**, 112563.
27 R. A. Wilson, J. Fernandez, R. O. Rocha, M. Marroquin-Guzman and J. D. Wright, Genetic evidence for Magnaporthe oryzae vitamin B_3 acquisition from rice cells, *Microbiology*, 2019, **165**, 1198.
28 C. Zhong, Y. Deng, W. Hu, J. Qiao, L. Zhang and J. Zhang, A review of electrolyte materials and compositions for electrochemical supercapacitors, *Chem. Soc. Rev.*, 2015, **44**, 7484–7539.
29 N. V. Plechkova and K. R. Seddon, Applications of ionic liquids in the chemical industry, *Chem. Soc. Rev.*, 2008, **37**, 123–150.
30 A. R. Neale, S. Murphy, P. Goodrich, C. Hardacre and J. Jacquemin, Thermophysical and Electrochemical Properties of Ethereal Functionalised Cyclic Alkylammonium-based Ionic Liquids as Potential Electrolytes for Electrochemical Applications, *ChemPhysChem*, 2017, **18**, 2040.
31 M. H. Cohen and D. Turnbull, Molecular transport in liquids and glasses, *J. Chem. Phys.*, 1959, **31**, 1164.
32 P. T. Callaghan, *Principles of nuclear magnetic resonance microscopy*, Clarendon press, Oxford, 1991.
33 J. E. Tanner, Use of the stimulated echo in NMR diffusion studies, *J. Chem. Phys.*, 1970, **52**, 2523.
34 Y. Zhao and D. G. Truhlar, Density functionals with broad applicability in chemistry, *Acc. Chem. Res.*, 2008, **41**, 157.
35 Y. Zhao, N. E. Schultz and D. G. Truhlar, Design of density functionals by combining the method of constraint satisfaction with parametrization for thermochemistry, thermochemical kinetics, and noncovalent interactions, *J. Chem. Theory Comput.*, 2006, **2**, 364.
36 M. J. Frisch, G. W. Trucks, H. B. Schlegel, G. E. Scuseria, M. A. Robb, J. R. Cheeseman, G. Scalmani, V. Barone, G. A. Petersson, H. Nakatsuji, X. Li, M. Caricato, A. V. Marenich, J. Bloino, B. G. Janesko, R. Gomperts, B. Mennucci, H. P. Hratchian, J. V. Ortiz, A. F. Izmaylov, J. L. Sonnenberg, D. Williams-Young, F. Ding, F. Lipparini, F. Egidi, J. Goings, B. Peng, A. Petrone, T. Henderson, D. Ranasinghe, V. G. Zakrzewski, J. Gao, N. Rega, G. Zheng, W. Liang, M. Hada, M. Ehara, K. Toyota, R. Fukuda, J. Hasegawa, M. Ishida, T. Nakajima, Y. Honda, O. Kitao, H. Nakai, T. Vreven, K. Throssell, J. A. Montgomery, Jr., J. E. Peralta, F. Ogliaro, M. J. Bearpark, J. J. Heyd, E. N. Brothers, K. N. Kudin, V. N. Staroverov, T. A. Keith, R. Kobayashi, J. Normand, K. Raghavachari, A. P. Rendell, J. C. Burant, S. S. Iyengar, J. Tomasi, M. Cossi, J. M. Millam, M. Klene, C. Adamo, R. Cammi, J. W. Ochterski, R. L. Martin, K. Morokuma, O. Farkas, J. B. Foresman and D. J. Fox, *Gaussian 16, Revision C.01*, Gaussian, Inc., Wallingford CT, 2016.
37 A. D. Becke, A new mixing of Hartree–Fock and local density-functional theories, *J. Chem. Phys.*, 1993, **98**, 1372.
38 C. Lee, W. Yang and R. G. Parr, Development of the Colle-Salvetti correlation-energy formula into a functional of the electron density, *Phys. Rev. B: Condens. Matter Mater. Phys.*, 1988, **37**, 785.
39 A. E. Reed, L. A. Curtiss and F. Weinhold, Intermolecular interactions from a natural bond orbital, donor–acceptor viewpoint, *Chem. Rev.*, 1988, **88**, 899.
40 H. Zhu, G. Huang, L. A. O'Dell and M. Forsyth, New insights into decoupled cation and anion transport and dynamic heterogeneity in a diethyl (methyl)(isobutyl) phosphonium hexafluorophosphate organic ionic plastic crystal, *J. Phys. Chem. Lett.*, 2021, **12**, 9853.
41 F. Makhlooghiazad, J. Guazzagaloppa, L. A. O'Dell, R. Yunis, A. Basile, P. C. Howlett and M. Forsyth, The influence of the size and symmetry of cations and anions on the physicochemical behavior of organic ionic plastic crystal electrolytes mixed with sodium salts, *Phys. Chem. Chem. Phys.*, 2018, **20**, 4721.
42 S. Das, A. Mondal and C. M. Reddy, Harnessing molecular rotations in plastic crystals: a holistic view for crystal engineering of adaptive soft materials, *Chem. Soc. Rev.*, 2020, **49**, 8878.

43 A. D. Nascimento, F. Caires, D. Gomes, A. Gigante and M. Ionashiro, Thermal behaviour of nicotinic acid, sodium nicotinate and its compounds with some bivalent transition metal ions, *Thermochim. Acta*, 2014, **575**, 212.

44 A. Marinković, S. Drmanić, B. Ž. Jovanović and M. Misić-Vuković, Investigations of the reactivity of pyridine carboxylic acids with diazodiphenylmethane in protic and aprotic solvents, Part I: pyridine mono-carboxylic acids, *J. Serb. Chem. Soc.*, 2005, **70**, 557.

45 J.-C. Hallé, J. Lelievre and F. Terrier, Solvent effect on preferred protonation sites in nicotinate and isonicotinate anions, *Can. J. Chem.*, 1996, **74**, 613.

46 I. A. Khan and F. U. Shah, Fluorine-free Ionic liquid-based electrolyte for supercapacitors operating at elevated temperatures, *ACS Sustainable Chem. Eng.*, 2020, **8**, 10212.

47 L. Zhu, J. Dong, Y. Ma, Y. Jia, C. Peng, W. Li, M. Zhang, K. Gong and X. Wang, Synthesis and investigation of halogen-free phosphonium-based ionic liquids for lubrication applications, *Tribol. Trans.*, 2019, **62**, 943.

48 D. R. Macfarlane, P. Meakin, J. Sun, N. Amini and M. Forsyth, Pyrrolidinium imides: a new family of molten salts and conductive plastic crystal phases, *J. Phys. Chem. B*, 1999, **103**, 4164.

49 F. U. Shah, S. Glavatskih, P. M. Dean, D. R. MacFarlane, M. Forsyth and O. N. Antzutkin, Halogen-free chelated orthoborate ionic liquids and organic ionic plastic crystals, *J. Mater. Chem.*, 2012, **22**, 6928.

50 Y. Shekibi, T. Rüther, J. Huang and A. F. Hollenkamp, Realisation of an all solid state lithium battery using solid high temperature plastic crystal electrolytes exhibiting liquid like conductivity, *Phys. Chem. Chem. Phys.*, 2012, **14**, 4597.

51 M. R. Yazdani, J. Etula, J. B. Zimmerman and A. Seppälä, Ionic cross-linked polyvinyl alcohol tunes vitrification and cold-crystallization of sugar alcohol for long-term thermal energy storage, *Green Chem.*, 2020, **22**, 5447.

52 E. Gómez, N. Calvar and Á. Domínguez, Thermal behaviour of pure ionic liquids, *Ionic Liq.: Curr. State of the Art*, 2015, **20**, 199.

53 G. M. Girard, M. Hilder, H. Zhu, D. Nucciarone, K. Whitbread, S. Zavorine, M. Moser, M. Forsyth, D. R. Macfarlane and P. C. Howlett, Electrochemical and physicochemical properties of small phosphonium cation ionic liquid electrolytes with high lithium salt content, *Phys. Chem. Chem. Phys.*, 2015, **17**, 8706.

54 M. Moreno, E. Simonetti, G. B. Appetecchi, M. Carewska, M. Montanino, G. T. Kim, N. Loeffler and S. Passerini, Ionic Liquid Electrolytes for Safer Lithium Batteries: I. Investigation Around Optimal Formulation, *ECS Trans.*, 2016, **73**, 67.

55 I. A. Khan, O. I. Gnezdilov, A. Filippov and F. U. Shah, Ion Transport and Electrochemical Properties of Fluorine-Free Lithium-Ion Battery Electrolytes Derived from Biomass, *ACS Sustainable Chem. Eng.*, 2021, **9**, 7769.

56 M. Galiński, A. Lewandowski and I. Stępniak, Ionic liquids as electrolytes, *Electrochim. Acta*, 2006, **51**, 5567.

57 A. Filippov, B. Munavirov, S. Glavatskih, F. U. Shah and O. N. Antzutkin, Diffusion of ions in phosphonium orthoborate ionic liquids studied by ^{1}H and ^{11}B pulsed field gradient NMR, *Front. Chem.*, 2020, **8**, 119.

58 M. Kakihana, S. Schantz and L. Torell, Raman spectroscopic study of ion–ion interaction and its temperature dependence in a poly (propylene-oxide)-based NaCF3SO3–polymer electrolyte, *Chem. Phys.*, 1990, **92**, 6271.

59 A. Savateev, C. Liedel, S. Tröger-Müller, A. S. de León, M. Antonietti and D. Dontsova, Halogen free 1,2,3-and 1,2,4-triazolide based ionic liquids: synthesis and properties, *Chem. Commun.*, 2017, **53**, 10192.

60 G. M. Girard, M. Hilder, D. Nucciarone, K. Whitbread, S. Zavorine, M. Moser, M. Forsyth, D. R. MacFarlane and P. C. Howlett, Role of Li concentration and the SEI layer in enabling high performance Li metal electrodes using a phosphonium bis (fluorosulfonyl) imide ionic liquid, *J. Phys. Chem. C*, 2017, **121**, 21087.

61 G. M. Girard, M. Hilder, N. Dupre, D. Guyomard, D. Nucciarone, K. Whitbread, S. Zavorine, M. Moser, M. Forsyth and D. R. MacFarlane, Spectroscopic characterization of the SEI layer formed on lithium metal electrodes in phosphonium bis (fluorosulfonyl) imide ionic liquid electrolytes, *ACS Appl. Mater. Interfaces*, 2018, **10**, 6719.

62 A. Soldatenkov, A. Temesgen and N. Kolyadina, Oxidation of heterocyclic compounds by permanganate anion, *Chem. Heterocycl. Compd.*, 2004, **40**, 537.

63 F. U. Shah, A. Holmgren, M. W. Rutland, S. Glavatskih and O. N. Antzutkin, Interfacial behavior of orthoborate ionic liquids at inorganic oxide surfaces probed by NMR, IR, and Raman spectroscopy, *J. Phys. Chem. C*, 2018, **122**, 19687.